

The effect of ion solvation on ion-induced nucleation – a generalized Thomson model

Roni Kroll* and Yoav Tsori†

Department of Chemical Engineering, Ben-Gurion University of the Negev, Beer Sheva 8510501, Israel.

(Dated: December 19, 2024)

We present a model for ion-induced nucleation, focusing on the effect of dissociated ions embedded in the fluid surrounding a charged core or colloid. The model includes the ions' direct electrostatic energy and preferential solvation. The integrated ions' free energy has two terms: The first can be short- or long-range, depending on their density. The second is proportional to the nucleus' volume and can shift the state from undersaturation to supersaturation at high ion concentration. The inclusion of the Gibbs transfer energies of ions in the free energy leads to a modified Poisson-Boltzmann equation for the potential around the core. The integrated ions' free energy is added to the fluids' interfacial and bulk terms to establish a generalized Thomson model. In the Debye-Hückel limit, the model is solved analytically, while in the nonlinear regime, it is solved numerically. The state diagram in the plane of saturation and core charge includes regions with a homogeneous phase, electropretting, metastable vapor, metastable nucleus, and spontaneous nucleation states. The lines separating these regions depend sensitively on the preferential solvation. Our model shows nucleation asymmetry to the sign of the nucleus' charge. This sign asymmetry is due to the Gibbs transfer energies of ions.

I. INTRODUCTION

Nucleation is a process where a stable phase emerges from a metastable state. It occurs in crystallization, melting, and boiling in physical, chemical and biological systems.[1] Nucleation depends on the microscopic, molecular, details, and therefore nucleation rates are difficult to obtain.[2] Classical nucleation theory is a continuum approach that uses the capillary assumption to describe the incumbent mesoscopic nucleus and the metastable phase by their bulk properties.[3–5] The theory assumes an infinitely sharp interface between phases and expresses the phenomenological free energy curve as a function of nucleus size R . [6, 7] Heterogeneous nucleation around small colloidal particles, e.g., aerosols in the atmosphere,[8–11] typically reduces the energy barrier between the phases and increases the corresponding transition rates.[12, 13] When a charged particle is embedded in vapor, a dielectrophoretic force acts on the fluid, aiding liquid condensation near the particle. The force and electrostatic potential decay as the inverse distance from the particle. Thomson's model incorporates this effect by adding a term proportional to the particle's charge squared into the classical nucleation theory.[14, 15] Indeed, experiments show that ion-induced nucleation, taking place in the presence of charged molecular clusters, is significantly enhanced. [16–18]

In a recent work, we extended the Thomson model to describe nucleation around charged particles in fluids containing dissolved ions, considering only the electrostatic forces.[19] In such fluids, dissociated ions lead to screening of the potential characterized by the Debye length. We found that the existence of ions lowers the energy barrier for nucleation. In the limit of high ionic strengths, the field is screened over a short length scale, and the effect of the charged particle is proportional to its *surface*. At negligible salt content, the behavior becomes identical to the Thomson model.

The term preferential ion solvation relates to the different ability of ions to dissolve in different solvents. Ion-specific effects are evident in the Hofmeister series and are well-studied.[20–22] Ammonium, sulfuric acid, and highly oxidized biogenic vapors are among the studied ions.[23–25] In liquid mixtures, the preferential solvation of ions depends on several parameters, such as the type of noncovalent bonds, ion size, and polarity.[26, 27] Preferential solvation affects several properties, such as surface tension and phase transitions.[28, 29] The ionic preference is quantified by the Gibbs transfer energy required for an ion to move from one phase to another.

The influence of charge sign on ion-induced nucleation has been extensively studied both experimentally and theoretically. Wilson's pioneering work demonstrated that nucleation is more pronounced around negative ions than positive ones.[30] For organic compounds such as dibutylphthalate, cations were found to promote nucleation more than anions, whereas the opposite trend was observed for nucleation of n -propanol around inorganic seed aerosol.[17, 31] Recent research has shown no clear sign preference for sub-3 nm particles and suggests that the parameter important in this size range is not the electrical sign but the chemical composition.[32] Several theoretical studies have attempted to elucidate the origin of sign symmetry-breaking using Monte Carlo and molecular dynamics simulations and density functional theory, but the conclusions were not definitive. [33–37]

Here, we generalize our previous work and look at the importance of ion solvation to nucleation. The free energy of the ions is composed of their entropy, electrostatic interactions, and preferential solvation. Ionic solvation appears as a *volume* term, and thus its effect occurs far from the particle. The ions' contribution is added to the classical surface tension and bulk terms in the energy to yield the Gibbs energy difference for nucleation. We show that core charge-asymmetric nucleation can be the result of an asymmetry between the Gibbs solvation energies of cations and anions.

* krollr@post.bgu.ac.il.

† tsori@bgu.ac.il.

II. MODEL DESCRIPTION

Figure 1 illustrates a spherical charged particle (colloid) with a uniform surface charge density σ and radius R_1 , surrounded by two immiscible fluids. Due to dielectrophoretic forces, the polar fluid is in contact with the colloid, while farther away the nonpolar phase is present. The system is spherically symmetric and the sharp interface between the two fluids is at $r = R$, where r is the distance from the core's center. The relative permittivities of the polar and nonpolar fluids are ϵ_p and ϵ_{np} . Ions are present in both phases but have a larger affinity to the polar phase. The preferential solvation of the ions is quantified by the Gibbs transfer energy, reflecting the difference in the equilibrium ions solvation energies between two bulk solvents. In our study, it is defined as the solvation energy of an ion in the polar phase minus its solvation energy in the nonpolar phase. For example, the Gibbs transfer energy of a sodium ion from water to *n*-propanol is $\Delta G_t = 16.8 [kJ/mol]$ and for chloride ion it is $\Delta G_t = 25.5 [kJ/mol]$. [38]

Note that even without a charged particle, close to the critical point, the presence of ions “help” condensation of gas to liquid; they raise the critical temperature by an amount proportional to ΔG_t^2 . [39] In this work, we assume that the density and temperature are far from the critical point and therefore ignore this effect.

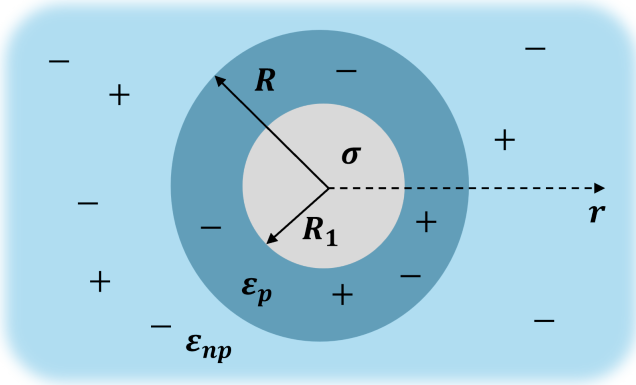


FIG. 1. Model illustration. A charged core particle (gray) with radius R_1 and surface charge density σ , surrounded by a polar phase (dark blue) with radius R and a nonpolar phase (light blue). The interface between the phases is infinitely thin. The system contains ions in both phases.

In our generalized Thomson model, the change in the Gibbs free energy for the formation of a dense, polar layer, at $r = R$ is

$$\Delta G = 4\pi\gamma R^2 - \frac{4}{3}\pi(R^3 - R_1^3)\Delta\mu + F_{\text{ions}}. \quad (1)$$

The first and second terms are the surface tension and bulk energy terms, respectively, where γ is the surface tension between the two phases, and $\Delta\mu$ is the difference in the chemical potential difference of the fluids per unit volume. When $\Delta\mu$ is positive, the mixture is supersaturated; when it is negative, it is undersaturated. The third term is the added energy due to

the presence of the ions and the charged core. The dissolved ions are assumed to be point-like and monovalent. We write F_{ions} as a volume integral of the entropy, solvation, and electrostatic energy densities as

$$F_{\text{ions}} = \int \left\{ k_B T [n^+ (\ln(v_0 n^+) - 1) + n^- (\ln(v_0 n^-) - 1)] + (H(r-R) - 1/2)(\Delta u^+ n^+ + \Delta u^- n^-) + \frac{1}{2} \epsilon \epsilon_0 (\nabla \psi)^2 - \mu^+ n^+ - \mu^- n^- \right\} d\mathbf{r}, \quad (2)$$

where k_B is the Boltzmann constant, T is the absolute temperature, v_0 is a volume comparable to the ion size, and H is the Heaviside step function. ψ represents the electrostatic potential while n^\pm denote the density profiles of anions and cations, all of which are dependent on r . μ^\pm are the chemical potentials of the ions, ϵ_0 is the permittivity of the vacuum and ϵ is the relative dielectric constant. The dimensionless parameters Δu^\pm quantify the Gibbs transfer energies. For the sodium and chloride ions in *n*-propanol, they are $\Delta u^+ \approx 7$ and $\Delta u^- \approx 10$, respectively.

In the regular Thomson model (no ions in the fluids), F_{ions} reduces to the integral over the electrostatic energy density only. Here, minimization of the free energy with respect to the cation and anion densities yields the Boltzmann distributions

$$n^\pm = n_0 e^{-\Delta u^\pm (H(r-R)-1) \mp \frac{e\psi}{k_B T}}, \quad (3)$$

with n_0 being the ion density at $r \rightarrow \infty$ where $\psi = 0$. We start by setting the Gibbs transfer energies equal for the anion and cation, $\Delta u^+ = \Delta u^- = \Delta u$, but relax this assumption later.

In spherical symmetry, the electrostatic potential satisfies the modified Poisson-Boltzmann equation

$$\psi_i'' + \frac{2}{r} \psi_i' = \frac{2en_0 e^{-\Delta u(H(r-R)-1)}}{\epsilon_i \epsilon_0} \sinh\left(\frac{e\psi}{k_B T}\right), \quad (4)$$

where $i=p$ or $i=np$ for either the polar or nonpolar phases.

The boundary conditions are as follows: Gauss's law determines the electric field on the colloid's surface, $\psi_p'(r=R_1) = -\sigma/\epsilon_0\epsilon_p$. At the interface, the electrostatic potential and displacement field are continuous: $\psi_p(r=R) = \psi_{np}(r=R)$ and $\epsilon_p \psi_p'(r=R) = \epsilon_{np} \psi_{np}'(r=R)$, and far away from the charged colloid the potential decays to zero, $\psi_{np}(r \rightarrow \infty) = 0$.

When the ion densities in Eq. (3) are substituted in Eq. (2), the dimensionless energy of the ions can be written as

$$\frac{F_{\text{ions}}}{4\pi k_B T} = \tilde{n}_0 \int \left\{ 2e^{-\Delta u(H(\tilde{r}-\tilde{R})-1)} (\tilde{\psi} \sinh(\tilde{\psi}) - \cosh(\tilde{\psi})) + \epsilon_i \tilde{\lambda}_0^2 (\tilde{\nabla} \tilde{\psi})^2 \right\} \tilde{r}^2 d\tilde{r}, \quad (5)$$

where $\tilde{\psi} = e\psi/k_B T$ and $\tilde{n}_0 = n_0 R_1^3$. The “vacuum Debye length” is defined with the permittivity of the vacuum as $\lambda_0 = (\epsilon_0 k_B T / 2n_0 e^2)^{1/2}$, and all lengths with “ $\tilde{\sim}$ ” sign are scaled by R_1 .

III. DEBYE-HÜCKEL LIMIT

In the Debye-Hückel limit, $\tilde{\psi} \ll 1$, the Poisson-Boltzmann equation (4) can be linearized to yield

$$\tilde{\psi}_i'' + \frac{2}{\tilde{r}} \tilde{\psi}_i' - \frac{1}{\tilde{\lambda}_i^2} \tilde{\psi}_i = 0, \quad (6)$$

where the Debye lengths in the polar and nonpolar phases are defined by

$$\lambda_p^2 = \frac{\epsilon_p}{e\Delta u} \lambda_0^2, \quad \lambda_{np}^2 = \epsilon_{np} \lambda_0^2, \quad (7)$$

and their scaled versions are $\tilde{\lambda}_i = \lambda_i/R_1$. Note that the exponential dependence of λ_p on Δu can reduce it significantly. The analytical solution is a combination of Yukawa potentials[19]

$$\begin{aligned} \tilde{\psi}_p &= \tilde{\sigma} \tilde{a}_p \frac{e^{\tilde{r}/\tilde{\lambda}_p}}{\tilde{r}} + \tilde{\sigma} \tilde{b}_p \frac{e^{-\tilde{r}/\tilde{\lambda}_p}}{\tilde{r}}, & 1 \leq \tilde{r} \leq \tilde{R}, \\ \tilde{\psi}_{np} &= \tilde{\sigma} \tilde{b}_{np} \frac{e^{-\tilde{r}/\tilde{\lambda}_{np}}}{\tilde{r}}, & \tilde{r} \geq \tilde{R}, \end{aligned} \quad (8)$$

where $\tilde{\sigma} = \sigma e R_1 / (k_B T \epsilon_0)$. The boundary condition at $\tilde{r} \rightarrow \infty$ eliminates the diverging exponential in $\tilde{\psi}_{np}$. The boundary conditions lead to a system of three linear equations with three unknown parameters, \tilde{a}_p , \tilde{b}_p , and \tilde{b}_{np} , that can readily be solved.

Once these coefficients are determined, the energy F_{ions} in Eq. (2) can be written analytically by

$$\frac{F_{\text{ions}}}{4\pi k_B T} = -\frac{2}{3} \tilde{n}_0 (\tilde{R}^3 - 1) (e^{\Delta u} - 1) + p_\sigma h(\tilde{R}). \quad (9)$$

The first term is the volume contribution of the solvation energy. It expresses a driving force that prefers a polar phase with condensed ions. It is linear in Δu for small values of Δu . The second term is the electrostatic energy, where $p_\sigma = \sigma^2 R_1^3 / 2k_B T \epsilon_0$ is the dimensionless ratio between the electrostatic energy stored in a sphere of radius R_1 and the thermal energy. The value of p_σ can significantly vary; for example, when σ corresponds to 8 unit charges evenly distributed over a surface of a sphere with $R_1 = 2$ nm, at room temperature $p_\sigma \approx 70$, whereas for a radius of $R_1 = 50$ nm, $p_\sigma \approx 3$.

$h(\tilde{R})$ above is a function of the nucleus size given by[19]

$$\begin{aligned} h(\tilde{R}) &= \epsilon_p \left[\tilde{a}_p^2 e^{2\tilde{r}/\tilde{\lambda}_p} (1/\tilde{\lambda}_p - 1/\tilde{r}) - \tilde{b}_p^2 e^{-2\tilde{r}/\tilde{\lambda}_p} (1/\tilde{\lambda}_p + 1/\tilde{r}) \right. \\ &\quad \left. - 2\tilde{a}_p \tilde{b}_p / \tilde{r} \right]_{\tilde{r}=1}^{\tilde{r}=\tilde{R}} + \epsilon_{np} \tilde{b}_{np}^2 e^{-2\tilde{R}/\tilde{\lambda}_{np}} (1/\tilde{\lambda}_{np} + 1/\tilde{R}). \end{aligned} \quad (10)$$

This Debye-Hückel expression is valid for small surface charges. Its dependence on \tilde{R} can be strong or weak.

The total Gibbs nucleation energy Eq. (1) can now be written in dimensionless form as

$$\begin{aligned} \frac{\Delta G}{4\pi k_B T} &= \\ p_\gamma \tilde{R}^2 &- (\tilde{R}^3 - 1) \left(p_\mu + \frac{2}{3} \tilde{n}_0 (e^{\Delta u} - 1) \right) + p_\sigma h(\tilde{R}), \end{aligned} \quad (11)$$

where $p_\gamma = \gamma R_1^2 / k_B T$ and $p_\mu = \Delta \mu R_1^3 / 3k_B T$.

At the limit of high salt concentration, $\tilde{\lambda}_p \ll 1$, the electric field is screened over the short distance $\tilde{\lambda}_p$, and $h(\tilde{R})$ tends to $h(\tilde{R}) \approx \tilde{\lambda}_p / \epsilon_p$ for $\tilde{R} > 1 + \tilde{\lambda}_p$. In this limit, the $p_\sigma h(\tilde{R})$ term in Eq. (12) is independent of \tilde{R} and plays the role of a surface term, i.e., the energy ΔG is an *effective* surface tension:

$$\frac{\Delta G}{4\pi R_1^2} = \gamma_s + \frac{\sigma^2 \lambda_p}{2\epsilon_0 \epsilon_p}, \quad (12)$$

where we added the bare surface tension between the liquid and the solid colloid γ_s . The correction to the bare surface tension scales with Δu as $\sim \lambda_p \propto e^{-\Delta u/2}$.

In the opposite limit of low salt concentration, $\tilde{\lambda}_i \rightarrow \infty$, the electrostatic term becomes

$$p_\sigma h(\tilde{R}) \approx p_\sigma \left[-\frac{1}{\epsilon_p} \left(\frac{1}{\tilde{R}} - 1 \right) + \frac{1}{\epsilon_{np} \tilde{R}} \right], \quad (13)$$

which is identical to the Thomson expression for dielectric fluids.

We note that the volume term in Eq. (12) ($\propto \tilde{R}^3 - 1$) is strong and long-range at high salt content; it leads to a renormalization of the supersaturation p_μ . Indeed, by combining the p_μ and $\sim \tilde{n}_0$ terms, one can write an *effective* chemical potential difference as

$$\mu_{\text{eff}} = \mu + 2k_B T n_0 (e^{\Delta u} - 1). \quad (14)$$

The second term on the right-hand side is of order $k_B T$ and can be large due to the exponential dependence on Δu .

In the next section, we solve the nonlinear problem numerically and obtain the energy for higher values of σ .

IV. NUMERICAL RESULTS

When the Debye-Hückel limit does not hold, we solve Eq. (4) numerically, with the charge density in the boundary condition at $\tilde{r} = 1$ determined by p_σ . We set values for the Debye length in vacuum, λ_0 , and the Bjerrum length in a vacuum, $l_{B0} = e^2 / \epsilon_0 k_B T$, which is the distance at which the thermal energy equals the Coulombic interaction of two unit charges. This indirectly determines the bulk ion density n_0 via $n_0 = 1/2l_{B0}\lambda_0^2$.

For the results in this section, we used $l_{B0}/R_1 = 70$, $\lambda_0/R_1 = 5$, and core with radius $R_1 \approx 10$ nm, and therefore the ion concentration is $n_0 \approx 5 \times 10^{-9}$ M. For the values $\epsilon_p = 80$ and $\Delta u = 2$ (see figures below), we find that $\lambda_p > l_{B0}$. Ion-ion correlations are thus small and the use of the mean-field Poisson-Boltzmann approach is justified.

Potential profiles for a given nucleus of size $R = 2R_1$ are presented in Fig. 2(a). The profiles $\psi(r)$ are continuous; the electric field $E = -\psi'(r)$ is discontinuous across the interface due to the jump in permittivity. The inset shows that with increasing values of Δu (increase in the affinity of ions to the polar phase at $r < R$) the surface potential, ψ_s , decreases. The corresponding ion distributions are presented in Figs. 2(b) and

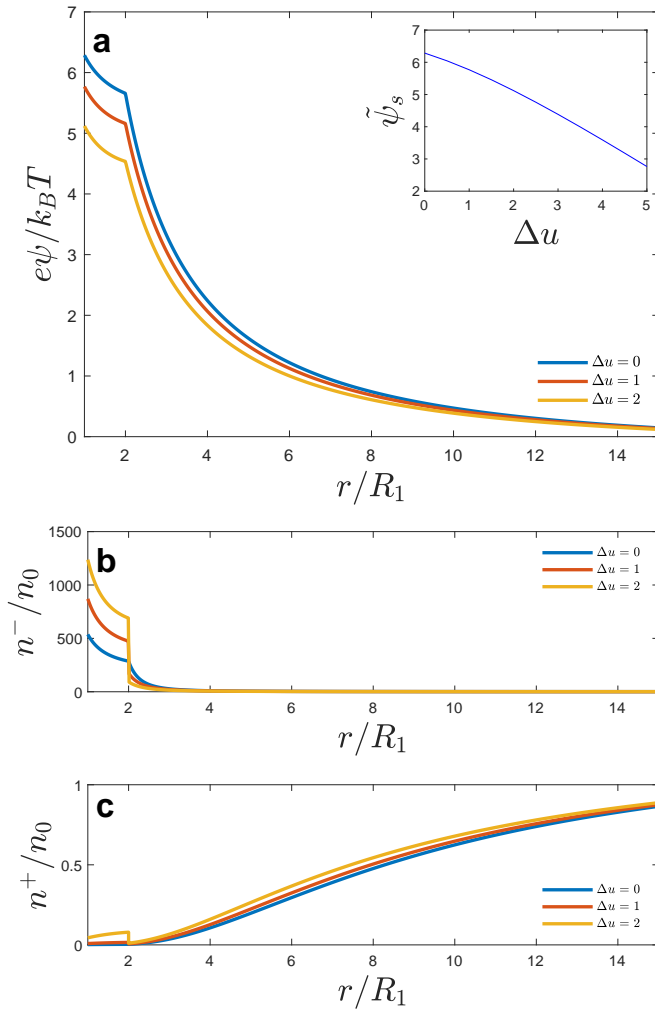


FIG. 2. (a) Dimensionless electrostatic potential profiles for different values of Δu , calculated numerically from Eq. (4). The inset shows the dimensionless surface potential $\tilde{\psi}_s = e\psi(r=R_1)/k_B T$, as a function of Δu . (b) Anion and (c) cation density profiles from Eq. (3). In (b), the high anion density at small r/R_1 is due to the assumption of point-like ions. In all parts of the figure, the nucleus' radius is $R = 2R_1$, where R_1 is the core radius, $p_\sigma = 80$, $\lambda_0/R_1 = 5$, $l_{B0}/R_1 = 70$, $\epsilon_p = 80$ and $\epsilon_{np} = 6$.

2(c). The densities are continuous across the interface in the absence of preferential solvation ($\Delta u = 0$). However, when the ions are preferentially miscible in the polar phase $\Delta u > 0$, their density in the polar phase increases, accompanied by a jump occurring at the interface. This kink results from an effectively chemical potential difference between the phases. The interface separates unequal quantities of the ions in the fluids, similar to the Donnan potential.[40] The kink disappears in models where the density of the fluid varies smoothly across the interface.[29] Although the value of preferential solvation of the anions and cations is similar, the difference between their density in the condensed phase is due to the positive sign of the core charge.

To obtain the ions' energy F_{ions} as a function of interface

location \tilde{R} , we substitute the potential profiles for different values of \tilde{R} into Eq. (5). We subtract the energy of a charged sphere surrounded by the nonpolar phase only, $F_{\text{ions}}(\tilde{R} = 1)$. The curves are presented in Fig. 3(a) for different Δu values. When $\Delta u = 0$, $F_{\text{ions}}(\tilde{R})$ monotonically decreases with \tilde{R} . When Δu increases, the ions' preferential solvation further reduces the energy, promoting the growth of the polar phase. An inflection point in the energy curves appears due to the large contribution of the volume term to the energy from a certain nucleus size (yellow line).

In Fig. 3(b), the total Gibbs energy profiles from Eqs. (1) and (5), including the surface tension and bulk energies, are shown. The dashed line is the energy curve for classical nucleation when the colloid is uncharged, $p_\sigma = 0$. Clearly, the presence of a charged colloid, $p_\sigma > 0$, significantly reduces the nucleation energy barrier. Additionally, a slight decrease in the size of the critical radius is observed. A local minimum appears in ΔG at small values of \tilde{R} . This corresponds to a metastable state of a nucleus with a finite size. When Δu is increased, the size of the metastable nucleus grows, and its energy decreases. Figures. 3(c) and 3(d) are similar to parts a-b, but with a higher value of ϵ_{np} . In this case, fewer ions are accumulated in the polar phase and the ions' energy, while still decreasing with \tilde{R} , does so more moderately. Consequently, the decrease in the energy barrier is smaller, and there are no metastable states in these parameter values.

The energy barrier, ΔG^* , is the difference between the maximum and local minimum values in the ΔG curves. The reduction of ΔG^* as a function of increasing Δu is presented in Fig. 4(a). This reduction can significantly accelerate nucleation, recalling that the nucleation rate depends exponentially on ΔG^* : $\sim \exp(-\Delta G^*/k_B T)$. Figure 4(b) shows the size of the metastable radius, R_m , as a function of Δu . Although the values of the metastable nuclei radius sizes presented here are minimal, they can be much larger closer to the critical temperature of the fluids.[41]

We now turn to investigate the effect of fluid saturation, as given by the parameter p_μ . When $p_\mu < 0$, the fluid is undersaturated and surrounded only by a nonpolar phase. $p_\mu = 0$ is the coexistence (binodal) value, and when $p_\mu > 0$, the fluid is supersaturated. Figure 5(a) shows the Gibbs nucleation curves for varying supersaturation values. ΔG for an undersaturated term is represented by the blue line, where the nucleation energy increases with the nucleus size due to the positive surface tension and bulk terms. Under these conditions, the electrostatic energy is insufficient to create a nucleus. For a positive value of p_μ , a local minimum appears at small \tilde{R} values and a maximum at larger \tilde{R} s. An increase in p_μ reduces the energy barrier until, at some point, it disappears. This is the value of the “electrostatic spinodal”, defined by $\Delta G^* = 0$, or, equivalently, by the existence of \tilde{R} for which $\Delta \tilde{G}''(\tilde{R}) = \Delta \tilde{G}'(\tilde{R}) = 0$. The electrostatic spinodal is a generalization of the regular spinodal curve for spontaneous nucleation due to the presence of the charged core and ions. Figure 5(b) compares ΔG curves for two different saturation values and two values of Δu . When $p_\mu = 0$, the blue curves indicate that an increase in Δu leads to the appearance of a finite-sized polar nucleus. The orange lines describe a supersaturated fluid, $p_\mu = 50$, where

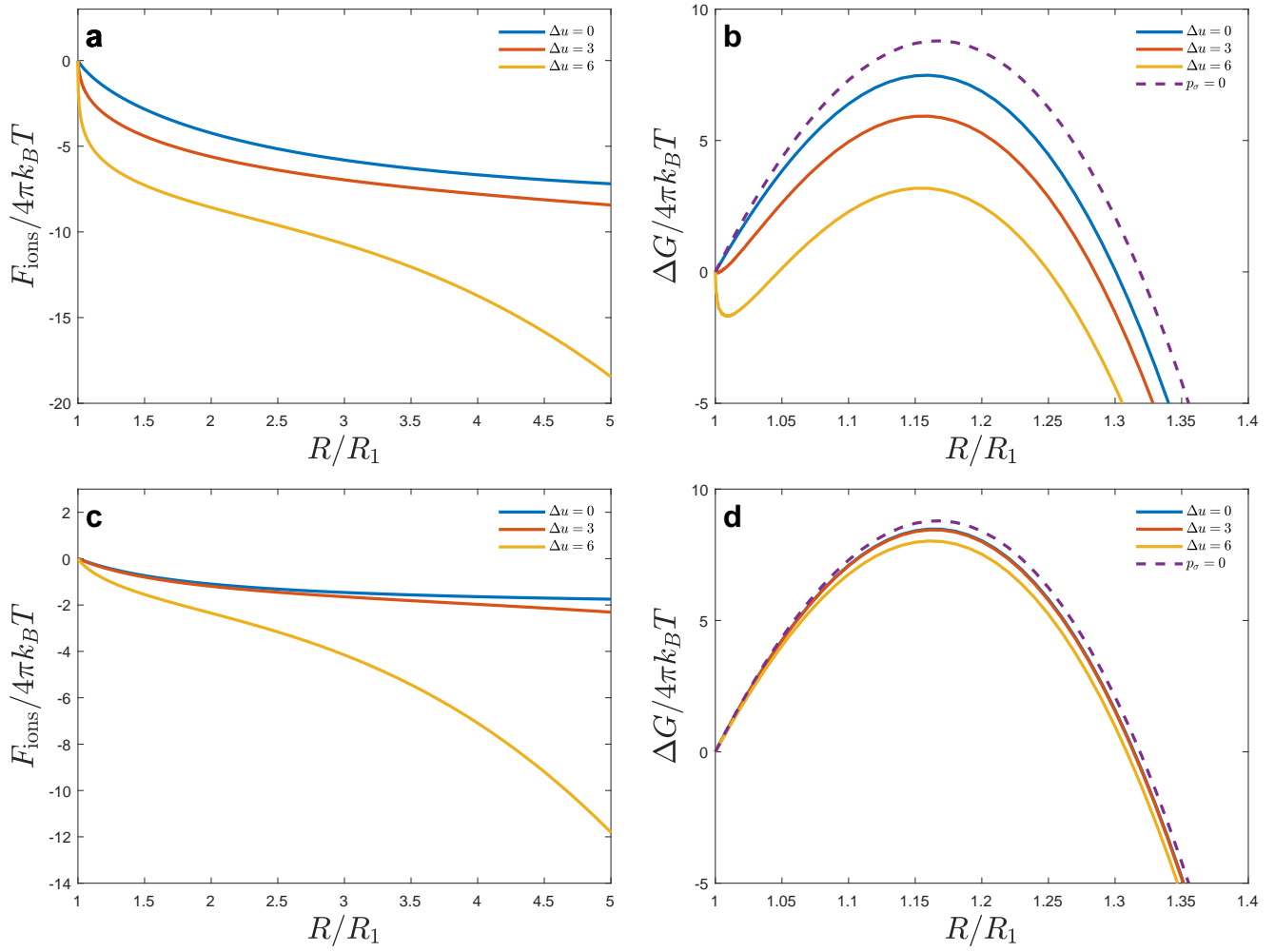


FIG. 3. The free energy of the ions $F_{\text{ions}}/4\pi k_B T$ (a) and the Gibbs nucleation energy $\Delta G/4\pi k_B T$ (b), obtained numerically, against the scaled nucleus radius R/R_1 (R_1 is the core radius), with $\epsilon_p = 80$ and $\epsilon_{\text{np}} = 6$. Figures (c) and (d) are similar, but calculated for a higher permittivity of the nonpolar phase $\epsilon_{\text{np}} = 25$. We used $p_\sigma = 80$, $p_\gamma = 350$, $p_\mu = 200$, $\lambda_0/R_1 = 5$, and $l_{B0}/R_1 = 70$.

the increase in Δu shifts the radius of the metastable nucleus to larger values and decreases the nucleation barrier.

Based on the ΔG curves, one can construct a state diagram in the saturation–colloid charge ($p_\mu - p_\sigma$) plane. Two such state diagrams are shown in Fig. 6 for $\Delta u = 3$ (a) and $\Delta u = 6$ (b). Each region in the state diagrams corresponds to a different Gibbs nucleation profile. In the blue region, where p_μ is negative and p_σ is not large, the fluids are in a state of one nonpolar phase. The electro-rewetting zone [orange, Fig. 6(b)] is the region where the fluid is undersaturated while the colloid’s charge is large enough that field-induced demixing occurs, leading to a finite-sized nucleus. The stability line separates these two regions and is defined as $\partial\Delta\tilde{G}/\partial\tilde{R}|_{\tilde{R}=1} = 0$. This line enters the supersaturated region ($p_\mu > 0$). At its two sides, the metastable region is divided into the metastable vapor region (purple), where $\Delta G(\tilde{R})$ does not have a local minimum at $\tilde{R} > 1$, and the metastable polar nucleus region (yellow). Spontaneous nucleation occurs at sufficiently large values of p_μ , green region. It is separated from the other two

regions by the “electrostatic spinodal” line. When p_σ tends to zero, the electrostatic spinodal tends to the value of the regular spinodal.

The increase in Δu dramatically changes the stability line, enlarging the electro-rewetting and metastable nucleus regions. That is, a larger value of Δu induces a finite-sized nucleus, whether stable or metastable. At the parameter values chosen, the limit between super- to undersaturation is not noticeable because, in Eq. (12), $\tilde{n}_0(e^{\Delta u} - 1)$ is of order 0.1.

We examine the effect of salt concentration by varying the values of $\tilde{\lambda}_0$. State diagrams in the $p_\mu - \tilde{\lambda}_0$ plane are shown in Figs. 7(a) and 7(b) for $\Delta u = 3$ and $\Delta u = 6$, respectively, with a fixed value of $p_\sigma = 80$. The stability line shifts significantly due to the dependence on Δu . In the absence of a charged core, phase transition occurs with no barrier below the regular spinodal line. In the presence of charged particle this line becomes the electrostatic spinodal. When this line is crossed by decreasing p_μ , a metastable minimum exists with a nucleation barrier. Electro-rewetting is promoted for the stronger

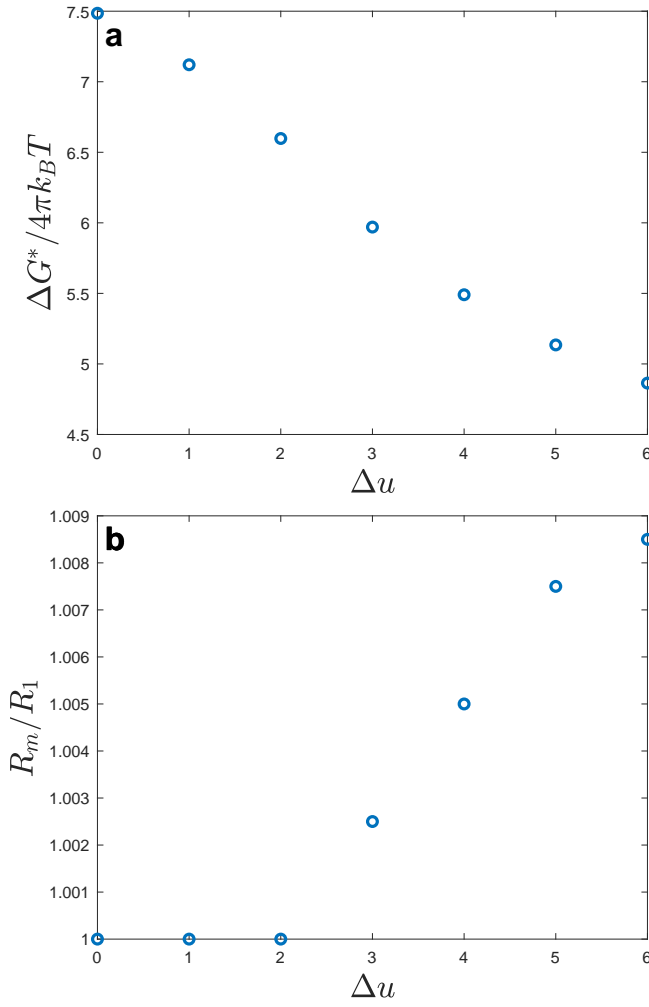


FIG. 4. (a) The dimensionless nucleation barrier $\Delta G^*/4\pi k_B T$ and (b) the radius of the metastable nucleus, R_m/R_1 vs Gibbs transfer energy value Δu . We used $p_\sigma = 80$, $p_\gamma = 350$, $p_\mu = 200$, $\lambda_0/R_1 = 5$, $l_{B0}/R_1 = 70$, $\epsilon_p = 80$ and $\epsilon_{np} = 6$.

solvation preference, especially at small $\tilde{\lambda}_0$ values (high salt content). The electrostatic spinodal is displaced to the left relative to the $\Delta u = 3$ case, with a $\approx 12\%$ shift compared to the regular spinodal (dashed gray line).

In the theoretical limit of exceedingly large salt concentrations ($\tilde{\lambda}_0 \rightarrow 0$), spontaneous nucleus growth happens for any value of p_μ , as the nucleation barrier completely disappears. Around $\tilde{\lambda}_0 \approx 3$, the Bjerrum length is equal to the Debye length of the polar phase; therefore, for smaller values, the theory should be extended to incorporate ion-ion correlations and finite-size effects.[42–44] Recent works demonstrated increased screening length when a Kirkwood transition occurs. [45–47] This increase is similar to an effective increase in λ_0 , and would have little effect in Fig. 7(a); in Fig. 7(b) it would shift the boundary between the one-phase and electro-pretwetting phases and would leave intact the other boundaries.

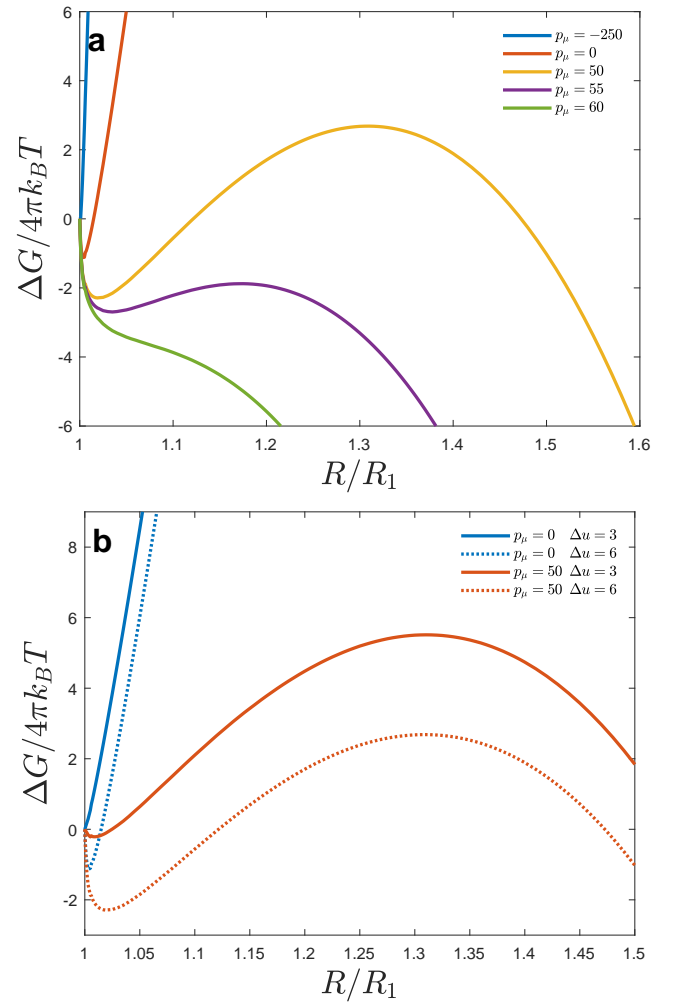


FIG. 5. (a) Gibbs energy profiles for different values of p_μ and $\Delta u = 6$. (b) Comparison between Gibbs energy profiles with two values of Δu and two values of p_μ . We used $p_\sigma = 80$, $p_\gamma = 100$, $\lambda_0/R_1 = 5$, $l_{B0}/R_1 = 70$, $\epsilon_p = 80$ and $\epsilon_{np} = 6$.

A. Asymmetry in the Gibbs transfer energy

We now remove the symmetry assumption in the Gibbs transfer energy, and calculate the Gibbs nucleation profiles where $\Delta u^+ \neq \Delta u^-$. In this case, Eq. (2) can be written as the following dimensionless expression

$$\frac{F_{\text{ions}}}{4\pi k_B T} = \tilde{n}_0 \int \left\{ -e^{-\Delta u^+ (H(\tilde{r}-\tilde{R})-1)-\tilde{\psi}(\tilde{\psi}+1)} + e^{-\Delta u^- (H(\tilde{r}-\tilde{R})-1)+\tilde{\psi}(\tilde{\psi}-1) + \epsilon_i \tilde{\lambda}_0^2 (\tilde{\nabla}\tilde{\psi})^2} \right\} \tilde{r}^2 d\tilde{r}, \quad (15)$$

where the potential profiles are again found from the modified Poisson-Boltzmann equation, which now includes the difference in Δu . The sign of the core charge determines whether anions or cations are in excess in the polar phase near the core's surface. In the case of asymmetric Δu s, this means the Gibbs nucleation energy curves $\Delta \tilde{G}(\tilde{R})$ depend on the core's charge. We calculated $\Delta \tilde{G}(\tilde{R})$ when $\Delta u^+ = 6$ for the cations

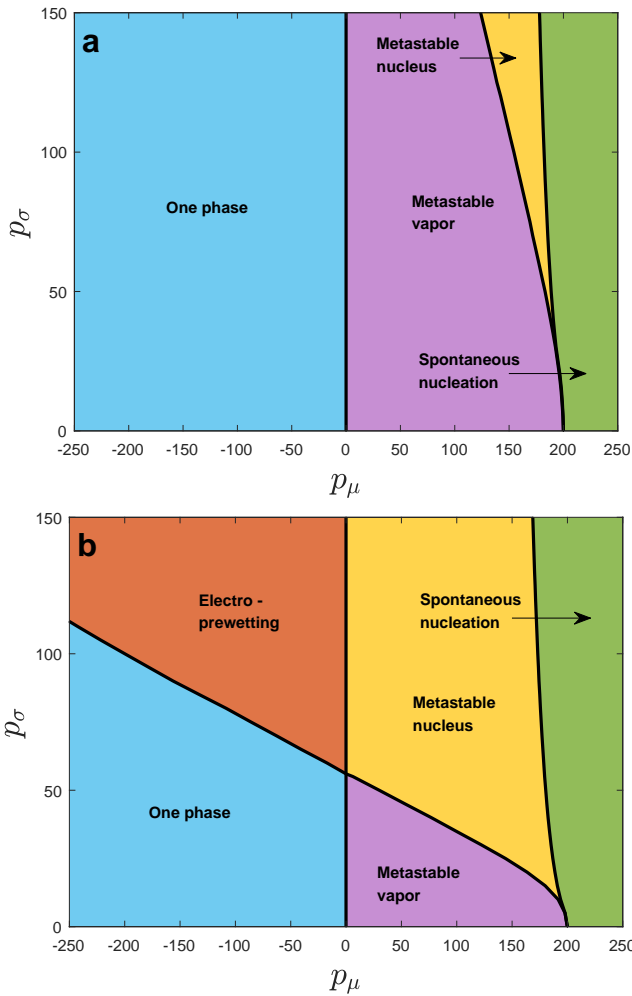


FIG. 6. State diagram in the p_μ - p_σ (saturation-core charge) plane for $\Delta u = 3$ (a), and $\Delta u = 6$ (b). Note how ionic preferential solvation in (b) enlarges the electro-pretwetting region and shrinks the one-phase region. For supersaturated fluids, preferential solvation decreases the metastable region in favor of metastable nucleus. We used $p_\gamma = 300$, $\lambda_0/R_1 = 5$, $l_{B0}/R_1 = 70$, $\epsilon_p = 80$ and $\epsilon_{np} = 6$.

and $\Delta u^- = 3$ for the anions. We used both a positive and negative sign for the core particle surface charge σ . The profiles are shown in Fig. 8. For the parameter values chosen, the energy barrier for the positive core charge is $\Delta G^*/k_B T \approx 5.9$ while for the negative one it is $\Delta G^*/k_B T \approx 4.9$. The nucleation rate almost triples due to the exponential dependence on the nucleation barrier.

V. SUMMARY AND CONCLUSIONS

We propose a simple mesoscopic model to describe nucleation induced by a charged core in polar fluids. The model applies to liquid/liquid coexistence and to a lesser extent to liquid/vapor systems. The solid spherical core is uniformly charged and surrounded by two layers of fluids separated by a thin interface, as is appropriate for a system far from its criti-

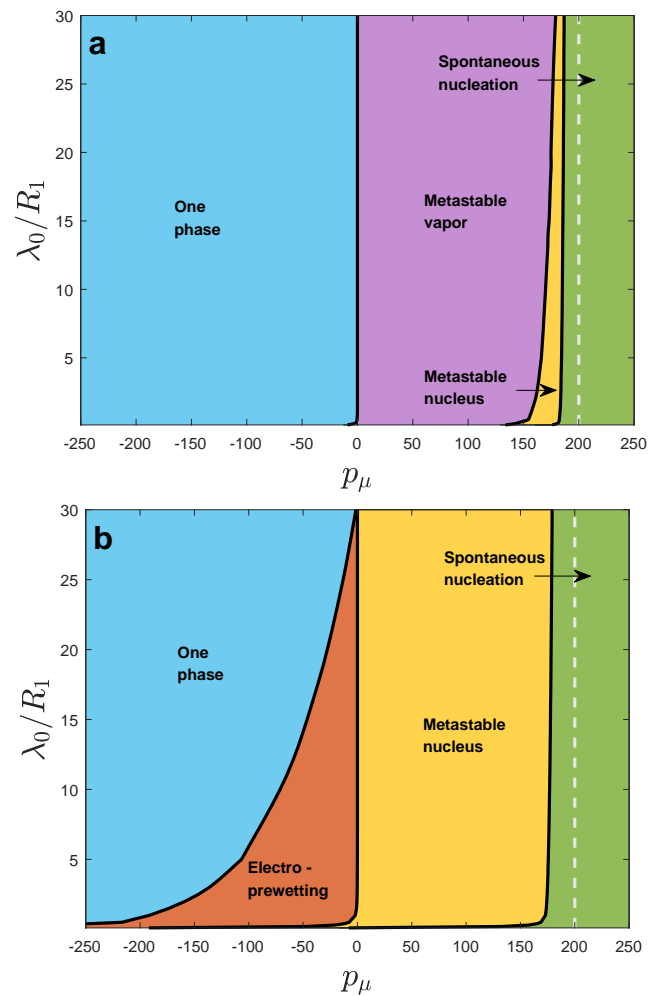


FIG. 7. State diagram in the p_μ - $\tilde{\lambda}_0$ (saturation-Debye length) plane for $\Delta u = 3$ (a), and $\Delta u = 6$ (b). The dashed gray line represents the value of the regular spinodal, calculated by the classical nucleation theory. We used $p_\gamma = 300$, $p_\sigma = 80$, $l_{B0}/R_1 = 70$, $\epsilon_p = 80$ and $\epsilon_{np} = 6$.

cal point. The fluids' properties are characterized by their bulk values. The main novelty of the present work is the inclusion of the ions' preferential solvation and electrostatic energy into the nucleation energy. The electrostatic potential around the colloid obeys a modified Poisson-Boltzmann equation. The equation is solved analytically for small charges and numerically otherwise. Once the potential is known, the ionic contribution is calculated and added to the interfacial and bulk energies to yield the total Gibbs free energy of nucleation.

The Thomson model for purely dielectric fluids shows that the energy barrier for nucleation decreases in the presence of a core-charged particle. As we show, in polar fluids, the solvation energy of ions amplifies this tendency despite the screening of the core charge. The colloid potential *decreases* monotonically with Δu . The state diagram in the plane of saturation and core charge is found from the Gibbs energy profiles. We show that preferential solvation changes considerably the lines separating the various regions—one phase,

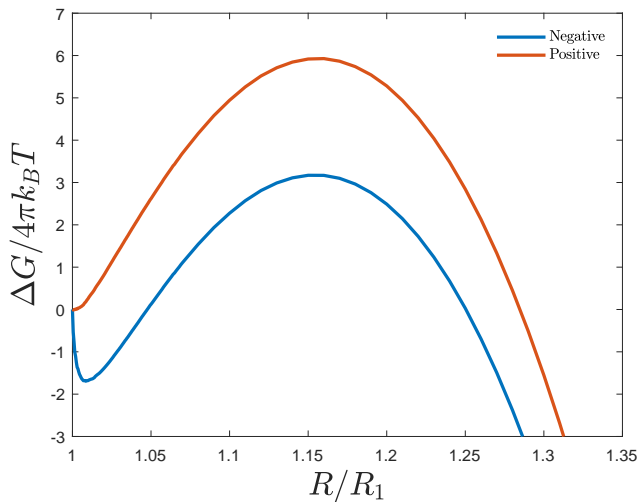


FIG. 8. Gibbs nucleation energy profiles for a positive and negative core charge sign (red and blue, respectively). The Gibbs solvation parameters are $\Delta u^+ = 6$ and $\Delta u^- = 3$, so in both plots, the cation's affinity to the polar phase is stronger than the anion's. We used $p_\gamma = 350$, $\lambda_0/R_1 = 5$, $l_{B0}/R_1 = 70$, $\epsilon_p = 80$ and $\epsilon_{np} = 6$.

electro-prewetting, metastable vapor, metastable nucleus, and spontaneous nucleations, see Fig. 6. In the phase diagram, the electrostatic spinodal separates the regions of metastable nucleus and the spontaneous nucleation. Upon crossing it, the energy barrier for nucleation disappears. In the absence of charge, this line becomes identical with the classical spinodal in bulk systems. In addition, differences in the preferential solvations of cations and anions, incorporated in the model using specific values of Δu^+ and Δu^- , may explain the asymmetry in nucleation rates between positive and negative cores. [9, 48]

Our continuum model uses point-like ions and predicts nucleus-charge sign asymmetry, and this is not found in experiment with sub-3nm particles.[32] This can be due to the finite-ions size and other effects. For example, the solvation energy and permittivity can vary on the nanometer scales, and ion complexation with other ions or solvent molecules is an intricate ion-specific process. Small clusters of ions and solvent molecules can act as the charged particle used in our model, though their shape will deviate from a perfect sphere. A possible multi-scale approach for future studies could be the integration of molecular dynamics or density functional theory simulations at these small scales with our continuum model to provide a comprehensive view of the nucleation process.

The current model assumes that the nucleating particles are spherical. Deviations from spherical symmetry could significantly modify the nucleation energies and rates and should be studied. A similar effect could occur with geometrically

spherical particles with inhomogeneous surface charge distribution.

The expression for nucleation in the presence of ions Eq. (12) is our main analytical result. The preferential solvation of ions reduces the energy barrier, assisting nucleation. Our previous work has shown that when a sufficiently large quantity of ions is present, without preferential solvation, screening of the core particle's electric charge results in a behavior similar to that of classical nucleation theory, only with a renormalized interfacial tension between the polar fluid and the particle's surface.[19] A similar effect occurs when $\Delta u > 0$, where $p_\sigma h(\tilde{R})$ reduces to a surface effect, see Eq. (12).

Preferential ion solvation appears explicitly in the volume term $\sim (\tilde{R}^3 - 1)$ in Eq. (12) as a term that renormalizes the value of p_μ , i.e., ions shift the location of the binodal curve. This shift is equivalent to a change of the chemical potential, Eq. (14). This shift can be quite large due to the exponential dependence $\sim \exp(\Delta u)$, recalling that in some liquids and ions Δu can be of order 10.[26]

When the Bjerrum length is large, for example, when the nonpolar phase is vapor, the model should include ion correlations. In addition, the dependence of the Gibbs transfer energies and the liquid's dielectric constants on ion density should be considered where relevant.[49, 50] For systems close to the critical point, the electric field gradients lead to notable deviations from the coexistence line even in the absence of ions [51–53] and the resulting first- and second-order phase transitions [41, 54] should be described using the density functional theory.[55–59]

It is reasonable to assume that a salt with a large affinity Δu can accelerate nucleation not only by reducing the energy barrier of a single nucleus but also through the coalescence of numerous metastable nuclei. At large distances, these nuclei repel because they are similarly-charged. At small distance, however, coalescence could occur if capillary forces are sufficiently strong. It can be interesting to look at the coalescence of such droplets in multi-particle theory or simulation. Moreover, it is intriguing whether such coalescence could occur in the electro-prewetting region of the state diagram. Antagonistic ions, where the cation prefers one phase, and the anion prefers the other, can have consequences to nucleation. For such ions, the anions and cations partition across the interface, reducing the surface tension between liquids, and this may further increase the nucleation rates.[60, 61]

ACKNOWLEDGMENTS

We are grateful for financial support by the Israel Science Foundation via Grant No. 332/24.

[1] D. Kashchiev. *Nucleation*. Elsevier, 2000.

[2] G. C. Sosso, J. Chen, S. J. Cox, M. Fitzner, P. Pedevilla, A. Zen, and A. Michaelides. Crystal nucleation in liquids: Open ques-

- tions and future challenges in molecular dynamics simulations. *Chem. Rev.*, 116(12):7078–7116, 2016.
- [3] M. Volmer and A. Weber. Keimbildung in übersättigten gebilden. *Zeitschrift für Physikalische Chemie*, 119U(1):277–301, 1926.
- [4] R. Becker and W. Döring. Kinetische behandlung der keimbildung in übersättigten dämpfen. *Annalen der Physik*, 416(8):719–752, 1935.
- [5] J. Frenkel. Statistical theory of condensation phenomena. *J. Chem. Phys.*, 7(3):200–201, 1939.
- [6] S. Karthika, T. K. Radhakrishnan, and P. Kalaichelvi. A review of classical and nonclassical nucleation theories. *Cryst. Growth Des.*, 16(11):6663–6681, 2016.
- [7] F. F. Abraham. *Homogeneous nucleation theory*, volume 263. Elsevier, 1974.
- [8] E. R. Lovejoy, J. Curtius, and K. D. Froyd. Atmospheric ion-induced nucleation of sulfuric acid and water. *J. Geophys. Res.*, 109(D8), 2004.
- [9] F. L. Eisele, E. R. Lovejoy, E. Kosciuch, K. F. Moore, R. L. Mauldin III, J. N. Smith, P. H. McMurry, and Kenjiro Iida. Negative atmospheric ions and their potential role in ion-induced nucleation. *J. Geophys. Res.*, 111(D4), 2006.
- [10] MD Petters and SM Kreidenweis. A single parameter representation of hygroscopic growth and cloud condensation nucleus activity. *Atmosp. Chem. Phys.*, 7(8):1961–1971, 2007.
- [11] Delphine K Farmer, Christopher D Cappa, and Sonia M Kreidenweis. Atmospheric processes and their controlling influence on cloud condensation nuclei activity. *Chem. Rev.*, 115(10):4199–4217, 2015.
- [12] A. Laaksonen, V. Talanquer, and D. W. Oxtoby. Nucleation: Measurements, theory, and atmospheric applications. *Ann. Phys. Chem.*, 46(1):489–524, 1995.
- [13] N. T. K. Thanh, N. Maclean, and S. Mahiddine. Mechanisms of nucleation and growth of nanoparticles in solution. *Chem. Rev.*, 114(15):7610–7630, 2014.
- [14] J. J. Thomson and G. P. Thomson. *Conduction of Electricity through Gases*. Cambridge University Press, Cambridge, 1933.
- [15] A. K. Shchekin and T. S. Podguzova. The modified Thomson equation in the theory of heterogeneous vapor nucleation on charged solid particles. *Atmos. Res.*, 101(3):493–502, 2011. International Conference on Nucleation and Atmospheric Aerosols (Part 2).
- [16] M. B. Enghoff, J. O. P. Pedersen, U. I. Uggerhøj, S. M. Palting, and H. Svensmark. Aerosol nucleation induced by a high energy particle beam. *Geophys. Res. Lett.*, 38(9), 2011.
- [17] M. Adachi, K. Okuyama, and J. H. Seinfeld. Experimental studies of ion-induced nucleation. *J. Aerosol Sci.*, 23(4):327–337, 1992.
- [18] J. Curtius, E. R. Lovejoy, and K. D. F. Atmospheric ion-induced aerosol nucleation. *Space Sci. Rev.*, 125(1-4):159–167, 2006.
- [19] R. Kroll and Y. Tsori. Nucleation by a charged particle in fluids containing salt. *J. Colloid Interface Sci.*, 650:13–18, 2023.
- [20] F. Hofmeister. Zur lehre von der wirkung der salze: Dritte mittheilung. *Archiv für experimentelle Pathologie und Pharmakologie*, 25:1–30, 1888.
- [21] Y. Zhang and P. S. Cremer. Interactions between macromolecules and ions: the hofmeister series. *Curr. Opin. Chem. Biol.*, 10(6):658–663, 2006.
- [22] K. P. Gregory, E. J. Wanless, G. B. Webber, V. S. J. Craig, and A. J. Page. The electrostatic origins of specific ion effects: quantifying the Hofmeister series for anions. *Chem. Sci.*, 12:15007–15015, 2021.
- [23] Hanitriainaina Rabeony and Pierre Mirabel. Experimental study of vapor nucleation on ions. *J. Phys. Chem.*, 91(7):1815–1818, 1987.
- [24] J. Almeida, S. Schobesberger, and A. et al Kürten. Molecular understanding of sulphuric acidamine particle nucleation in the atmosphere. *Nature*, 502:359–363, 2013.
- [25] J. Kirkby, J. Duplissy, and K. et al Sengupta. Ion-induced nucleation of pure biogenic particles. *Nature*, 533:521–526, 2016.
- [26] Y. Marcus. Preferential solvation. part 3.—binary solvent mixtures. *J. Chem. Soc. Faraday Trans. 1*, 85:381–388, 1989.
- [27] H. S. Chan and K. A. Dill. Solvation: Effects of molecular size and shape. *J. Chem. Phys.*, 101(8):7007–7026, 1994.
- [28] A. Onuki. Surface tension of electrolytes: Hydrophilic and hydrophobic ions near an interface. *J. Chem. Phys.*, 128(22):224704, 2008.
- [29] A. Onuki. Ginzburg-landau theory of solvation in polar fluids: Ion distribution around an interface. *Phys. Rev. E*, 73:021506, 2006.
- [30] C. T. R. Wilson and J. J. Thomson. Xi. condensation of water vapour in the presence of dust-free air and other gases. *Philosophical Transactions of the Royal Society of London. Series A, Containing Papers of a Mathematical or Physical Character*, 189:265–307, 1897.
- [31] P. M. Winkler, G. Steiner, A. Vrtala, H. Vehkamäki, M. Noppel, K. E. J. Lehtinen, G. P. Reischl, P. E. Wagner, and M. Kulmala. Heterogeneous nucleation experiments bridging the scale from molecular ion clusters to nanoparticles. *Science*, 319(5868):1374–1377, 2008.
- [32] J. Kangasluoma, A. Samodurov, M. Attoui, A. Franchin, H. Junninen, F. Korhonen, T. Kurtén, H. Vehkamäki, M. Sipilä, K. Lehtipalo, D. R. Worsnop, T. Petäjä, and M. Kulmala. Heterogeneous nucleation onto ions and neutralized ions: Insights into sign-preference. *J. Phys. Chem. C*, 120(13):7444–7450, 2016.
- [33] K. J. Oh, G. T. Gao, and Xiao. C. Zeng. Nucleation of water and methanol droplets on cations and anions: The sign preference. *Phys. Rev. Lett.*, 86:5080–5083, 2001.
- [34] E. Brodskaya, A. P. Lyubartsev, and A. Laaksonen. Investigation of water clusters containing oh- and h3o+ ions in atmospheric conditions. a molecular dynamics simulation study. *Phys. Chem. B.*, 106(25):6479–6487, 2002.
- [35] A. B. Nadykto, F. Yu, and J. Herb. Towards understanding the sign preference in binary atmospheric nucleation. *Phys. Chem. Chem. Phys.*, 10:7073–7078, 2008.
- [36] S. M. Kathmann, G. K. Schenter, and B. C. Garrett. Ion-induced nucleation: the importance of chemistry. *Phys. Rev. Lett.*, 94(11):116104, 2005.
- [37] Samuel J. Keasler, Hyunmi Kim, and Bin Chen. Sign preference in ion-induced nucleation: Contributions to the free energy barrier. *J. Chem. Phys.*, 137(17):174308, 11 2012.
- [38] Y. Marcus. Single ion Gibbs free energies of transfer from water to organic and mixed solvents. *Rev. Analyt. Chem.*, 5(1-2):53–137, 1980.
- [39] Y. Tsori and L. Leibler. Phase-separation in ion-containing mixtures in electric fields. *Proc. Natl. Acad. Sci.*, 104(18):7348–7350, 2007.
- [40] Frederick George Donnan. The theory of membrane equilibria. *Chem. Rev.*, 1(1):73–90, 1924.
- [41] R. Kroll and Y. Tsori. Liquid nucleation around charged particles in the vapor phase. *J. Chem. Phys.*, 155(17), 2021.
- [42] Y. Levin. Electrostatic correlations: from plasma to biology. *Rep. Prog. Phys.*, 65(11):1577, 2002.
- [43] R. M. Adar, T. Markovich, A. Levy, H. Orland, and D. Andelman. Dielectric constant of ionic solutions: Combined effects of correlations and excluded volume. *J. Chem. Phys.*, 149(5), 2018.

- [44] R. M. Adar, S. A. Safran, H. Diamant, and D. Andelman. Screening length for finite-size ions in concentrated electrolytes. *Phys. Rev. E*, 100(4):042615, 2019.
- [45] B. Rotenberg, O. Bernard, and J. P. Hansen. Underscreening in ionic liquids: a first principles analysis. *J. Phys.: Condens. Matter*, 30(5):054005, 2018.
- [46] S. W. Coles, C. Park, R. Nikam, M. Kanduč, J. Dzubiella, and B. Rotenberg. Correlation length in concentrated electrolytes: Insights from all-atom molecular dynamics simulations. *J. Phys. Chem. B*, 124(9):1778–1786, 2020.
- [47] E. O. Fetisov, C. J. Mundy, G. K. Schenter, C. J. Benmore, J. L. Fulton, and S. M. Kathmann. Nanometer-scale correlations in aqueous salt solutions. *J. Phys. Chem. Lett.*, 11(7):2598–2604, 2020.
- [48] Manuel Gamero-Castano and Juan Fernández de la Mora. Ion-induced nucleation: Measurement of the effect of embryo’s size and charge state on the critical supersaturation. *J. chem. Phys.*, 117(7):3345–3353, 2002.
- [49] D. Ben-Yaakov, D. Andelman, and R. Podgornik. Dielectric decrement as a source of ion-specific effects. *J. Chem. Phys.*, 134(7), 2011.
- [50] T. Markovich, D. Andelman, and R. Podgornik. Surface tension of electrolyte interfaces: Ionic specificity within a field-theory approach. *J. Chem. Phys.*, 142(4):044702, 2015.
- [51] L. D. Landau and E. M. Lifshitz. *Electrodynamics of continuous media*. Nauka (Moscow), 1957.
- [52] Y. Tsori, F. Tournilhac, and L. Leibler. Demixing in simple fluids induced by electric field gradients. *Nature*, 430:544–7, 2004.
- [53] R. Kroll and Y. Tsori. Phase lines in mean-field models with nonuniform external forces. *J. Chem. Phys.*, 157(23), 2022.
- [54] Y. Tsori. Electroprewetting near a flat charged surface. *Phys. Rev. E*, 104(5):054801, 2021.
- [55] J. Z. Wu. *Density functional theory for liquid structure and thermodynamics*. Springer, 2008.
- [56] P. Tarazona and R. Evans. A simple density functional theory for inhomogeneous liquids: Wetting by gas at a solid-liquid interface. *Mol. Phys.*, 52(4):847–857, 1984.
- [57] V. Talanquer and D. W. Oxtoby. Dynamical density functional theory of gas-liquid nucleation. *J. Chem. Phys.*, 100(7):5190–5200, 1994.
- [58] A. J. Archer and R. Evans. Dynamical density functional theory and its application to spinodal decomposition. *J. Chem. Phys.*, 121(9):4246–4254, 2004.
- [59] R. Okamoto and A. Onuki. Density functional theory of gas-liquid phase separation in dilute binary mixtures. *J. Phys.: Condens. Matter*, 28(24):244012, 2016.
- [60] R. Kroll and Y. Tsori. Surface tension in liquids containing antagonistic ions. *Soft Matter*, 16:2055–2064, 2020.
- [61] R. Kroll, M. Gottlieb, and Y. Tsori. Surface tension between liquids containing antagonistic and regular salts. *Eur. Phys. J. E*, 46, 2023.